Optik 125 (2014) 861–864

Contents lists available at ScienceDirect

Optik

journal homepage: www.elsevier.de/ijleo

High resolution optical image restoration for ground-based large telescope using phase diversity speckle

Shixue Zhang*, Bin Wang, Jinyu Zhao

Changchun Institute of Optics, Fine Mechanics and Physics, Chinese Academy of Sciences, Dongnanhu Road 3888, Changchun 130033, China

ARTICLE INFO

Article history:
Received 21 March 2013
Accepted 21 July 2013

Keywords:
Phase diversity speckle
Image restoration
Wave-front aberration
Phase estimation
Ground-based telescope

ABSTRACT

Phase diversity speckle (PDS) is an image restoration technique which is based on the idea of phase diversity (PD). It uses multi-frame short-exposure image sequence to calculate their corresponding wave-front information. Each image pair consists of two images collected by two cameras at the same time with one in focus and the other with known defocus value. Multi-frame processing can significantly improve the target signal to noise ratio, and decrease noise influence. In this paper, based on the principle of pupil Fourier imaging, by adjusting the pupil size, we get different scales of the optical point spread function (PSF). Also, we analysis different camera noise distribution channels, location differences and other factors to optimize the objective evaluation function, and this can reduce the computational complexity and improve the processing speed of image restoration. In the indoor environment, we build optical platform, and use multi-frame phase diversity speckle to make experiment under different turbulence conditions. The experimental results show that the image restoration effect of the proposed method is close to the diffraction limit.

1. Introduction

The performance of high-resolution ground-based telescope imaging is limited by atmospheric turbulence. Regardless of how much the telescope aperture is, optical resolution is limited to the level of 1 arc second. To meet the imaging requirements, the telescope should have capabilities of tracking moving target to ensure the moving target relatively static. This leads to one fact: during the transmission from the reflected light of the object, the atmospheric turbulences in the wavefront [1] caused special and temporal fluctuations, thus making the image had a serious degradation. Real-time adaptive optics technology can compensate for atmospheric turbulence. It is a more mature technology at present. However, the adaptive systems are complex and expensive, and the correct effect is based on observing conditions, object and system performance. In addition, since adaptive optics only corrects partial frequency components, the corrected images also need post-image processing.

Phase diversity method was first proposed by Gonsalves and Childlaw [2]. The main idea is to acquire two images simultaneously with one in focus and the other defocus, and calculate wavefront phase distribution with the knowledge of defocus value and restore the object. Paxman and others further improved the PD theory with the combination of speckle imaging techniques. They proposed the phase diversity speckle (PDS) method of collecting one pair or more of the short exposure image from both focal plane and defocus plane, and gave the mathematical model under Gaussian noise and Poisson noise, which greatly improves the PDS in the case of noise estimation accuracy. Vogel and others used inverse related theory to propose a fast numerical solution [3,4]. Löfdahl and others successfully applied the PDS theory to the solar observation, and obtained high-resolution images of the solar surface [5,6].

This paper, based on the above, uses a high-precision translation platform to move a high-speed cooling camera imaging system, and collects multi-frame short-exposure image from the focal plane and defocus plane, and uses defocus phase difference to estimate both object and wavefront phase. Meanwhile, we analyze noise distribution channels, location differences and other factors on different camera, and optimize the object evaluation function to reduce the computational complexity and improve the processing speed of image restoration.

2. PDS principles and models

Fig. 1 shows PDS image acquisition system with focal plane channel and defocus plane channel. In the defocus plane channel, a spectroscopic is placed and the amount of defocus is known. PDS image restoration can be regarded as an inverse problem [7] to solve the object and the wavefront phase with known turbulence. The use of multiple channels improves the ill-posed problems, and the

* Corresponding author. Tel.: +86 15043085135; fax: +86 431 84627071.
E-mail address: zhangsx@ciomp.ac.cn (S. Zhang).

0030-4026/$ – see front matter.
http://dx.doi.org/10.1016/j.ijleo.2013.07.110

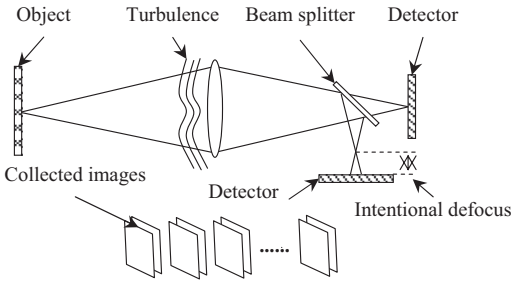

Fig. 1. Data-collection scheme for PDS imaging.

use of multi-frame short exposure images improves object signal to noise ratio.

2.1. Imaging model

Atmosphere and telescope basically compose the linear space-invariant system. In the non-coherent light illumination, the imaging formula of Gaussian noise model is as follows [8]:

$$d(x) = f(x) \times s(x) + n(x) \tag{1}$$

Where d is actual object image collected on the CCD, f is the ideal object image, s is point spread function, n is Gaussian noise, and x is coordinate on image plane.

With the condition of near-field, the point spread function is denoted as follows:

$$s(x) = \left| \mathcal{F}^{-1} \left\{ P(\upsilon) e^{i\phi(\upsilon)} \right\} \right|^2 \tag{2}$$

Where $\mathcal{F}^{-1}$ is inverse Fourier transform, υ is pupil plane coordinates, P is pupil function. ϕ is wave-front phase, which can be decomposed into a set of Zernike polynomials,

$$\phi(\upsilon) = \theta(\upsilon) + \sum_{m=4}^{M} \alpha_m Z_m(\upsilon) \tag{3}$$

Where α_m is mth coefficients of the polynomial, Z_m is mth Zernike polynomial base, θ is the known defocus phase.

2.2. Evaluation function

In the Gaussian noise model, the mean variance between the object and multi-channel image can be used as the likelihood function [9–11], and it can be expressed in the frequency domain as:

$$L(f, \{\alpha\}_t) = \frac{1}{2N} \sum_u \left(\sum_{t=1}^{T} \sum_{c=1}^{C} \left| D_{tc}(u) - F S_{tc}(u) \right|^2 + \gamma \left| F(u) \right|^2 \right) \tag{4}$$

Where u is the frequency domain coordinates, T and C are the number of frames and channels respectively, N is the total number of pixels of a single image, $\{\alpha\}_t$ t-frame Zernike coefficient to be solved. $\gamma \left| F(u) \right|^2$ is Tikhonov regularization term [3,4], which can improve the algorithm stability and convergence rate, where γ is the non-negative regular coefficients.

By the maximum likelihood estimation theory, the object estimation is a process that is separated with phase estimation to obtain object-independent evaluation function [10]. Among them, the object estimation formula is the middle process to derive the evaluation function with the Wiener filter form, and it can effectively reduce the noise.

$$L(\{\alpha\}_t) = \frac{1}{2N} \sum_u \left(\sum_{t=1}^{T} \sum_{c=1}^{C} \left| D_{tc} \right|^2 - \frac{\left| \sum_{t=1}^{T} \sum_{c=1}^{C} D_{tc} S_{tc}^* \right|^2}{\gamma + \sum_{t=1}^{T} \sum_{c=1}^{C} \left| S_{tc} \right|^2} \right) \tag{5}$$

$$F = \frac{\sum_{t=1}^{T} \sum_{c=1}^{C} D_{tc} S_{tc}^*}{\gamma + \sum_{t=1}^{T} \sum_{c=1}^{C} \left| S_{tc} \right|^2} \tag{6}$$

When evaluation function is determined, the image restoration process can be described as a nonlinear optimization extremum process. In this paper, we use simple constraints limited memory quasi-Newton method (L-BFGS-B) [12,13] that is suitable for large-scale variable optimization, and write C++ based software optimization platform. After a long test, the algorithm has better convergence efficiency.

2.3. The improvement of the objective function

During the iterative process of PD, when calculating the objective function and its partial derivatives, each individual S_{tc} should be calculated according to $\{\alpha\}_t$. And each S_{tc} requires Fourier transform of four double-precision calculations, which greatly increased the difficulty of hardware implementation of the algorithm PD. In addition, it reduces the parallel efficiency of hardware implementation, and increases data transfer between DSP and FPGA. Apart from this they are simple matrix-bit computing, and it is easy to use FPGA to implement. So in order to construct a PDS for hardware processing of the object function and its derivative, the key question is how to rewrite the solution function of S_{tc}.

As we all know, the set of Zernike polynomial functions is a complete set on the unit circle. And we can get the following equation:

$$H = P(\upsilon) e^{i\phi(\upsilon)} = \sum_{m=1}^{M} \beta_m Z_m(\upsilon) \tag{7}$$

Eq. (7) is also the basis of extended Zernike derivation. Where β_m is complex number, α_m in formula (3) is real number. So generalized pupil function on c channel of the t frame is

$$H_{tc} = P(\upsilon) e^{i\phi_t(\upsilon) + i\theta_c(\upsilon)} = \sum_{m=1}^{M} \beta_{tm} Z_m(\upsilon) e^{i\theta_c(\upsilon)} \tag{8}$$

Where $\theta_c(\upsilon)$ is the known fixed wavefront differences between channel 1 and channel c. Next we calculate its optical transfer function:

$$S_{tc} = \mathcal{F} \left(\left| \mathcal{F}^{-1} \left\{ H_{tc} \right\} \right|^2 \right) \tag{9}$$

$$S_{tc} = \sum_{m=1}^{M} \sum_{n=1}^{M} \beta_m \beta_n^* A_{mn} \tag{10}$$

$$A_{mnc} = \mathcal{F} \left\{ \mathcal{F}^{-1} \left[Z_m(\upsilon) e^{i\theta_c(\upsilon)} \right] \mathcal{F}^{-1} \left[Z_n(\upsilon) e^{i\theta_c(\upsilon)} \right]^* \right\} \tag{11}$$

A_{mn} can be calculated in the initialization process of PDS, even for a fixed PDS optical route, A_{mn} is the same, and a matrix can be stored in the FPGA as an constant. Then the calculation of the objective function during iterative process of PDS is simple to use formula (10) to obtain S_{tc}, and the polynomial suitable for parallel computing using FPGA circuit. The calculation of partial derivative

according to $\{\beta\}_t$ for the objective function is also simply a derivative of the polynomial. Next the each partial derivative equation according to each variable of the improved objective function is given:

$$\frac{\partial L}{\partial(\mathrm{Real}(\beta_{tn}))} = \frac{-1}{N}\mathrm{Real}\left(\sum_{x,y\in\chi}\sum_{c=1}^{C} R_{tcn}Q_{tc}\right) \tag{12}$$

$$\frac{\partial L}{\partial(\mathrm{Imag}(\beta_{tn}))} = \frac{-1}{N}\mathrm{Real}\left(\sum_{x,y\in\chi}\sum_{c=1}^{C} I_{tcn}Q_{tc}\right) \tag{13}$$

$$Q_{tc} = F^{*}D_{tc} - \left|F\right|^{2}S_{tc} \tag{14}$$

$$R_{tcn} = \sum_{m=1}^{M}\left(\beta_{tm}^{*}A_{nmc} + \beta_{tm}A_{mnc}\right) \tag{15}$$

$$I_{tcn} = \sum_{m=1}^{M} i\left(\beta_{tm}^{*}A_{nmc} - \beta_{tm}A_{mnc}\right) \tag{16}$$

As can be seen from the above formula, the calculation of partial derivatives on each independent variable of the objective function is the only polynomial operations. Next we should analyze this objective function.

The improvement of the objective function has the following advantages. (1) The calculations in computing the solution of PDS are all polynomial operations, to facilitate hardware implementation, and improve the parallelism solution of the objective function; (2) The objective function can handle different pupil transmittance of the optical system, the transmittance rate is actually the amplitude of $\sum_{m=1}^{M}\beta_m Z_m(\upsilon)$.

Also this improvement of the objective function has some drawbacks. (1) For practical project, the method is suitable for hardware implementation, but not suitable for running on the CPU. The computational complexity of the algorithm after improvement is $O(M^{*}M^{*}N)$, while the previous computational complexity is $O(N\log_2 N)$, where M is the number of Zernike coefficients selected in PDS calculation, N is the total number of pixels in the collected images. (2) The method actually obtains generalized pupil function, and the wavefront phase directly obtained by the generalized pupil function evaluation phase angle will have winding problem. The solution of phase winding can be difficult, for its residuals are not Gaussian distributed. (3) The number of parameters of the objective function after improvement may be much greater than before. Because for the situation that wave rate is the same through the pupil, the total number M1 of Zernike items of generalized pupil using $P(\upsilon)e^{i\sum_{m=4}^{M1}\alpha_m Z_m(\upsilon)}$ is less than the total number M2 of Zernike items generalized of pupil Zernike using $\sum_{m=1}^{M2}\beta_m Z_m(\upsilon)$, and each β is composed of real and imaginary parts.

Now what we are most concerned about is that, in practical engineering, how much of M2 can meet the requirement. The derivation of this problem will be very difficult, and depending on the wavefront of the rms value and the proportion of high-frequency components. By testing a lot of data, a M2 value of 200 can meet the requirement for the project. Considering the experience before, M2 has been enough to take 100. But even of this size, the CPU cannot achieve real-time calculation, a platform with FPGA and DSP is needed.

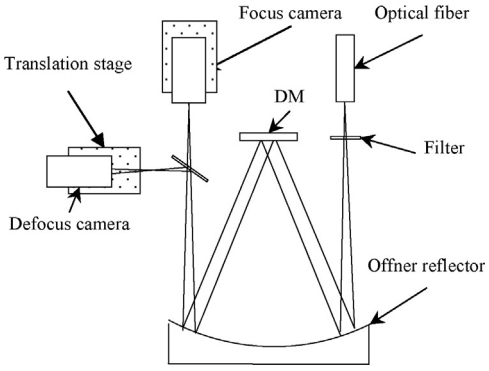

Fig. 2. Structure of experimental system.

3. Experimental system

We use the experimental system as in Ref. [14–15], and we implement a single-frame two-channel version of the program on CPU, M2 only takes value of 20.

We add a second camera, and use external trigger to synchronously acquire images on the first camera. In addition, in order to simulate atmospheric turbulence, we use a hair dryer to add disturbance to optical route. This is a commonly used indoor adaptive optics experimental method, which we can only do in current conditions.

The experimental system consists of the objective light source, disturbance model, images collection as shown in Fig. 2. Experimental platform layout is shown in Fig. 3.

4. Experimental results

In our experimental system, the focal length is 0.895 m, center wavelength is 635 nm, the pupil diameter (i.e. deformable mirror diameter) is 0.05 m, depth of focus is about 0.407 mm. Defocus value should be about 4 times the depth of focus, and the actual defocus value is 1.6 mm, fixed-focus phase PV value is about one wavelength. Camera pixel size is 16 μm, the optical system cut-off frequency of about 72 lines/mm; camera cut-off frequency is 31.25 lines/mm; use optical fiber as the object, at the same time each set of images from the focal plane and defocus plane take the area of 128 × 128, and exposure time is 20 ms.

We have made PDS operations from a single frame, three frames, and ten frames respectively, and made comparison of them.

As shown in Fig. 4, Fig. 4(a) is the first frame of the focal plane image of the image sequences. In the restored images, the resolution of the optical fiber has been significantly improved, and the outline is clearly visible between the particles. However, Fig. 4(b) shows that single-frame image restoration has serious ghosting, that is, wavefront calculation still has a relatively large error. In Fig. 4(c), the restored images with three frames are further improved than the single frame, but still it has a small amount of ghosting. While in Fig. 4(d), the restored image with ten frames has almost no ghosting. That is the wavefront error in each of the

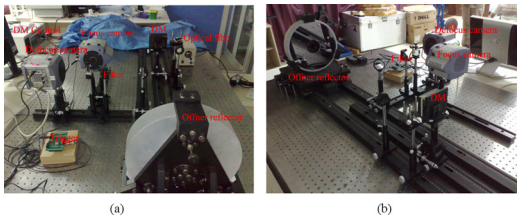

Fig. 3. Experimental layout.

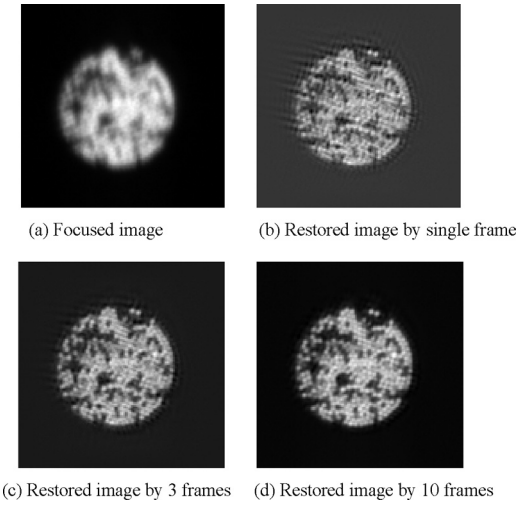

Fig. 4. Original images and result. (a) Focused image and (b) restored image by single frame. (c) Restored image by 3 frames and (d) restored image by 10 frames.

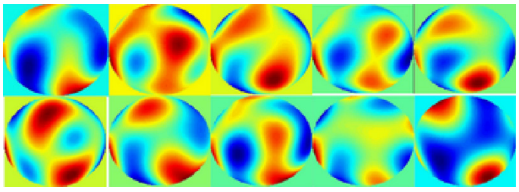

Fig. 5. Wave-front phases by 10 frames PDS.

ten frames wavefront error is less than the error of the corresponding frame with a single-frame wavefront calculation. Thus, image restoration with PD speckle imaging is better than the simple PD algorithm. Fig. 5 is the wave-front phase diagram calculated by PD speckle system using a continuous ten short exposure images, and their corresponding restored image is in Fig. 4(d).

5. Conclusion

This paper uses two external trigger mode cameras to achieve PDS dual-channel simultaneous acquisition. We analyze the problem of two cameras compared with a single camera. The clarity of restored image is significantly improved with number of frames increases. We validate the ability of the PDS algorithm in image resolution improvement; also the ability of PDS to restore the image is better than PD.

Acknowledgements

The authors would like to thank Department of Electro-Optical Detection, Changchun Institute of Optics, Fine Mechanics and Physics, Chinese Academy of Sciences, for providing raw images. The work was supported by the National High-Tech Research & Development Program of China (Grant No. 2008AA8080202).

References

[1] Y.H. Chen, L. Huang, L. Gan, Z.Y. Li, Wavefront shaping of infrared light through a subwavelength hole, Light Sci. Appl. 1 (2012) e26.
[2] R.A. Gonsalves, R. Childlaw, Wave-front sensing by phase retrieval, in: Applications of Digital Image Processing, Vol. 207, 1979, pp. 32–39.
[3] C.R. Vogel, Computational Methods for Inverse Problems, SIAM Press, Philadelphia, 2002.
[4] C.R. Vogel, T. Chan, R. Plemmons, Fast algorithms for Phase Diversity-Based Blind Deconvolution, Adaptive Optical System Technologies, Vol. 3353, SPIE, Kona, Hawaii, USA, 1998, pp. 994–1005.
[5] M.G. Löfdahl, T.E. Berger, R.S. Shine, et al., Preparation of a dual wavelength sequence of high-resolution solar photospheric images using phase diversity, Astrophys. J. 495 (1998) 965–972.
[6] M.G. Löfdahl, G.B. Scharmer, Wave-front sensing and image restoration from focused and defocused solar images, Astron. Astrophys. 107 (1994) 243–264.
[7] V.F. Paz, S. Peterhansel, K. Frenner, W. Osten, Solving the inverse grating problem by white light interference Fourier scatterometry, Light Sci. Appl. 1 (2012) e36.
[8] M.C. Roggemann, B.M. Welsh, Imaging Through Turbulence, CRC Press, Washington, 1996.
[9] R.G. Paxman, T.J. Schulz, J.R. Fienup, Joint estimation of object and aberrations by using phase diversity, J. Opt. Soc. Am. A9 (1992) 1072–1085.
[10] R.G. Paxman, J.H. Seldin, M.G. Löfdahl, et al., Evaluation of phase-diversity techniques for solar-image restoration, Astrophys. J. 466 (1996) 1087–1099.
[11] B.J. Thelen, R.G. Paxman, D.A. Carrara, et al., Maximum a posteriori estimation of fixed aberrations, dynamic aberrations, and the object from phase-diverse speckle data, J. Opt. Soc. Am. A16 (1999) 1759–1768.
[12] R.H. Byrd, P. Lu, J. Nocedal, et al., A Limited Memory Algorithm for Bound Constrained Optimization, Report NAM-08, EECS Department Northwestern University, 1994.
[13] C. Zhu, R.H. Byrd, P. Lu, et al., LBFGS-B: Fortran Subroutines for Large-Scale Bound Constrained Optimization. Report NAM-11, EECS Department, Northwestern University, 1994.
[14] J. Wang, Z. Wang, B. Wang, et al., Image restoration by phase-diversity speckle, Opt. Precision Eng. 19 (2011) 1165–1170 (in Chinese).
[15] J. Zhao, Z. Chen, B. Wang, et al., Parallelity improvement of object function for phase diversity, Opt. Precision Eng. 20 (2) (2012) 431–438 (in Chinese).